



HAL
open science

Metagenome-derived virus-microbe ratios across ecosystems

Purificación López-García, Ana Gutiérrez-Preciado, Mart Krupovic, Maria Ciobanu, Philippe Deschamps, Ludwig Jardillier, Mario López-Pérez, Francisco Rodríguez-Valera, David Moreira

► **To cite this version:**

Purificación López-García, Ana Gutiérrez-Preciado, Mart Krupovic, Maria Ciobanu, Philippe Deschamps, et al.. Metagenome-derived virus-microbe ratios across ecosystems. *The International Society of Microbiological Ecology Journal*, 2023, 17 (10), pp.1552-1563. 10.1038/s41396-023-01431-y . hal-04108767

HAL Id: hal-04108767

<https://hal.science/hal-04108767v1>

Submitted on 28 May 2023

HAL is a multi-disciplinary open access archive for the deposit and dissemination of scientific research documents, whether they are published or not. The documents may come from teaching and research institutions in France or abroad, or from public or private research centers.

L'archive ouverte pluridisciplinaire **HAL**, est destinée au dépôt et à la diffusion de documents scientifiques de niveau recherche, publiés ou non, émanant des établissements d'enseignement et de recherche français ou étrangers, des laboratoires publics ou privés.

Metagenome-derived virus-microbe ratios across ecosystems

5 **Purificación López-García^{1*}✉, Ana Gutiérrez-Preciado^{1*}, Mart Krupovic², Maria Ciobanu¹, Philippe Deschamps¹, Ludwig Jardillier¹, Mario López-Pérez³, Francisco Rodríguez-Valera³, David Moreira¹**

10 ¹ Ecologie Systématique Evolution, CNRS, Université Paris-Saclay, AgroParisTech, Gif-sur-Yvette, France

² Institut Pasteur, Université Paris Cité, CNRS UMR6047, Archaeal Virology Unit, Paris, France

15 ³ Departamento de Producción Vegetal y Microbiología, Universidad Miguel Hernández, Alicante, Spain

* These authors contributed equally to this work

20

✉ For correspondence, puri.lopez@universite-paris-saclay.fr

Abstract

It is generally assumed that viruses outnumber cells on Earth by at least tenfold. Virus-to-
25 microbe ratios (VMR) are largely based on counts of fluorescently labelled virus-like
particles. However, these exclude intracellular viruses and potentially include false positives
(DNA-containing vesicles, gene-transfer agents, unspecifically stained inert particles). Here,
we develop a metagenome-based VMR estimate (mVRM) that accounts for DNA viruses
across all stages of their replication cycles (virion, intracellular lytic and lysogenic) by using
30 normalised RPKM (reads per kilobase of gene sequence per million of mapped metagenome
reads) counts of the major capsid protein (MCP) genes and cellular universal single-copy
genes (USCGs) as proxies for virus and cell counts, respectively. After benchmarking this
strategy using mock metagenomes with increasing VMR, we inferred mVMR across different
biomes. To properly estimate mVMR in aquatic ecosystems, we generated metagenomes
35 from co-occurring cellular and viral fractions (>50 kDa-200 μ m size-range) in freshwater,
seawater and solar saltern ponds (10 metagenomes, 2 control metaviromes). Viruses
outnumbered cells in freshwater by ~13 fold and in plankton from marine and saline waters
by ~2-4 fold. However, across an additional set of 121 diverse non-aquatic metagenomes
including microbial mats, microbialites, soils, freshwater and marine sediments and
40 metazoan-associated microbiomes, viruses, on average, outnumbered cells by barely two-
fold. Although viruses likely are the most diverse biological entities on Earth, their global
numbers might be closer to those of cells than previously estimated.

45 **Introduction**

Viruses are strict molecular parasites that play crucial roles in ecosystems. They control host population sizes and contribute to biogeochemical nutrient cycling [1, 2], helping to maintain biodiversity through “*kill-the-winner*” strategies [3, 4]. They are also important players in evolution, exerting selective pressures on cell populations and triggering arms-race processes, fostering the evolution of genes and genomes and serving as vehicles for horizontal gene transfer [5]. Viruses are also enormously diverse, with new lineages being widely uncovered by metagenomic and metatranscriptomic approaches [6, 7]. It seems therefore natural to think that viruses are also very abundant, but their actual global number and how it compares to that of their hosts remains unclear.

55 Viruses are generally thought to be at least one order of magnitude more abundant than microbial cells on Earth [2, 8-10]. These abundance estimates are largely based on epifluorescence microscopy or flow cytometry (FCM) counts of virus-like particles (VLPs) and cells stained with nucleic acid dyes. These methods were originally applied to marine plankton, where measured virus-to-microbe ratios (VMR) frequently revolve, despite
60 substantial variation, around 10 (Ref. [1, 9, 11]). However, epifluorescence-based VLP counts exclude temperate viruses and are blind to intracellular lytic viruses during the eclipse phase of infection. Conversely, these methods can suffer from diverse false positives, including cell-DNA-containing membrane vesicles [12-15] or gene-transfer agents [10, 16] and, usually overlooked, non-specifically stained organic and/or mineral particles [17, 18].
65 The latter might be important confounding factors in high-density ecosystems such as sediments and soils, where cell and VLP detachment from the organic-mineral matrix is required prior to epifluorescence-based quantification [19]. VMR values are particularly disparate in sediments and soils [19-21] and broadly vary depending on the protocol used [22]. Several observations suggest that the VLP counts proportionally diminish with
70 increasing cell density [23, 24], although it has been hypothesized that lower VMR in cell-dense environments does not necessarily reflect low viral load but rather higher lysogenic prevalence [24]. However, while VMR seems to decline with increasing microbial cell densities, evidence for enhanced lysogeny remains ambiguous [25]. All these confounding factors challenge the accuracy of the existing VMR estimates and maintain uncertainty about
75 the actual viral load supported by cellular organisms across ecosystems. Hence, more reliable approaches for obtaining this ratio and deriving ecologically relevant comparisons across biomes are needed.

Here, we develop a metagenome-based strategy to estimate VMR (mVMR) for DNA viruses (RNA viruses cannot be targeted by this approach) across all stages of their viral replication cycles (viral particles –VP–, as well as intracellular lytic and lysogenic viruses). We first benchmark this method on mock metagenomes with increasing VMR. Then, we estimate mVMRs from *de novo* generated aquatic-system metagenomes comprising coexisting viral particles (VPs) and cell fractions (50 kDa - 200 μ m) and compare the obtained estimates with classical epifluorescence-derived estimates (fVMR). Finally, we estimate mVMR from 121 additional metagenomes across diverse ecosystem types, notably including high-density habitats. Our results show that mVMR are adequate proxies that can more realistically account for DNA virus:cell ratios in natural ecosystems than fVMR.

Materials and Methods

Metagenome-based counting of cells and viruses

To count cells, we used a set of 15 universal single-copy genes (USCGs; Table S1) highly conserved across the three cellular domains, including the reduced and often fast-evolving members of the Candidate Phyla Radiation (CPR, Patescibacteria) and the DPANN archaea. USCGs were identified via their PFAM motifs (Pfam-A database v3.1b2) [26] and searched in two datasets (Prokka-predicted genes and OrfM-predicted ORFs) with HMMER `hmmsearch` [27] v3.2.1 with the trust cut-off threshold. To assign relevant hits to taxa, they were analysed using `Diamond` [28] v0.9.25.126 against the NCBI non-redundant database formatted by Kaiju [29] v1.7.1: `kaiju_db_nr_euk.faa`, which contains all NCBI reference sequences for archaea, bacteria, eukaryotes and viruses. Best hits with more than 35% identity over at least 70% of query lengths were included in a best-hit table in kaiju-like output format using an *ad hoc* Perl script (`mimicKaijuOutput.pl`). They were then assigned to taxa using the kaiju script `addTaxonName`. Most genomes used to build the mock metagenomes had only one copy of the set of 15 USCGs (see below). Accordingly, the average of counts for the selected 15 USCGs in metagenomes represents an adequate proxy for individual cell counts. Five of the chosen ribosomal protein markers in the list of USCGs are known to have two copies in halophilic archaea and, accordingly, we divided by two haloarchaeal counts for them prior to averaging total counts. To estimate the number of viruses in metagenomes, we used as a proxy genes encoding major capsid proteins (MCPs). We used a total of 132 HMM profiles covering the MCPs of (almost) all known families of DNA viruses or viruses with intermediate DNA stages (ssDNA, dsDNA, RT-DNA) that

infect bacteria, archaea and eukaryotes, including some relatively recently described viral groups, such as Yaraviridae [30] or Autolykiviridae [31] (but not the even more recently identified Mirusviruses [32], which might remain less well detected). For the analysis of the mock and planktonic metagenomes (see below), we specifically included HMM profiles of environmentally abundant marine viruses discovered by metagenomics (e.g., viruses of MGII Euryarchaeota, MGI Thaumarchaeota, marine Thermoplasmata, etc) and, to capture viruses of the rest of metagenomes, we built specific HMM profiles. For this, metagenome contigs assigned to viruses whose MCPs were not captured by existing HMM were used to build new HMM profiles. For reference, MCP sequences representing each family of DNA viruses, homologs were retrieved from the UniRef database, filtered to 30% sequence identity (3 iterations, inclusion value of $E=1e-3$) and aligned using hhblits [33], part of the hhsuite package 3.3.0 (Ref. [34]). The resulting alignments were converted to profile HMMs using hmmbuild included in the HMMER package v3.3.2 (Ref. [35]). Most genes retrieved with the MCP HMMs were functionally annotated as either capsid or hypothetical proteins and were assigned to viruses by our taxonomic assignment pipeline. However, several HMMs retrieved genes annotated as (diverse) encapsulins and simultaneously assigned to bacteria; these HMMs preferentially retrieving bacterial encapsulins were excluded from further analyses. MCP HMM profiles that consistently retrieved genes assigned to cellular taxa and had clear cellular functions were discarded. A final set of 132 MCP HMMs (Table S2) was retained and used to search against all the Viral Ref Seq database (NCBI) using HMMER hmmsearch [27] v3.2.1 with an E value of $1e-11$ threshold. In the case of genes attributed to different MCPs, the gene IDs were hashed and the MCP assignment with the lowest e-value was retained. Since multiple MCPs can occasionally be found in large viral genomes, we counted only one MCP per contig and considered that, under these constraints, 1 MCP represents 1 virus. To assess mVMR in mock metagenomes, nucleotide sequences of identified cellular USCGs and viral MCPs were indexed with Bowtie [36] v2.3.5.1 and the original mock metagenome reads mapped back onto them. Mapped reads were retrieved with Samtools [37] v1.9 and, for each gene, the Reads Per Kilobase (of gene sequence) per Million of mapped metagenome reads (RPKM) were calculated using *ad hoc* Perl scripts, allowing normalization for gene length and sample sequencing depth. Subsequently, we selected the USCG that recovered the most RPKMs per metagenome and the sum of MCP RPKMs to obtain normalised mVMRs. For an easier visualization of the proportion of viruses per microbial cell, we further normalised the viral RPKMs with respect to the number of cells (cell value = 1). Plots were generated with *ad hoc* R scripts using the ggplot2 package [38].

Mock metagenomes

Ten mock metagenomes were built from a selection of 50 viral and 50 cellular genomes retrieved from the NCBI reference sequence database RefSeq (<https://www.ncbi.nlm.nih.gov/>) and GTDB (<https://gtdb.ecogenomic.org/>). Genomes were selected to partly mimic a simplified microbial community of marine plankton that included viruses, archaea, bacteria and eukaryotes (Table S3). To simulate the output of Illumina HiSeq sequencing, all genomic sequences were fragmented into 10 million reads of 100 bp using cMessi [39]. Eight mock metagenomes were built by varying the relative abundance of the viral vs. cellular reads in a range from 10 cells per viral genome to 125 viral genomes per microbial cell (V001M10 to V125M01; names reflect the virus:microbe ratio). The two additional metagenomes contained either none of the selected viral genomes (V000M01) or only viral sequences (V001M00; Fig. 1A). The generated reads were assembled with Metaspades [40] v3.13.1 with default parameters and k-mer iteration cycles of “21,25,31,35,41,45,51,55”. Assembly statistics are shown in Table S4. Gene annotation was performed on assembled contigs with Prokka [41] v1.14.5 in metagenome mode (contigs >200 bp). In parallel, to more exhaustively identify gene/protein domains, all ORFs were predicted with OrfM [42] (Table S5). Both annotation methods (Prokka and OrfM) produced very similar results (Fig. S1), albeit Prokka performed slightly better for high VMR values (Fig. 1B-C). We thus chose to display the contig-based Prokka annotation in subsequent analyses.

Water sampling, filtration, DNA purification and mixes for metagenome sequencing

Samples from the Mediterranean Sea were collected on 27/02/2019 at 20 m (MedS) and 40 m (MedD) depth in the water column (bottom depth 220 m) from a previously studied site off the Alicante coast (38°4'6.64"N, 0°13'55.18"W) [43]. The CTD (Seabird) data showed a typically winter-mixed water column, with homogeneous temperature (14.8°C), pH (8.4) and dissolved oxygen (8.5 ppm) throughout at least 60 m depth. Water was collected through a hose with a 200- μ m Nitex mesh-capped end attached to the CTD and directly pumped onto a serial filtration system mounted with 20, 5 and 0.22 μ m pore-size polycarbonate filters (Millipore). Biomass-containing filters were frozen on dry ice for transport to the laboratory prior to immediate DNA purification. The resulting <0.2 μ m filtrate (200 l) was recovered in 50-l carboys and used for tangential filtration, which took place overnight on arrival at 4°C (cold room) using 6 Vivaflow200 filtration units (Sartorius) operating in two parallel series.

The volume of concentrated viral fractions (>50 kDa) was further reduced using Amicon
180 Ultra 15 ml Centrifugal Filters (Merck-Millipore) prior to phenol/chloroform extraction.
Water samples (10 l) with increasing salt concentration (6%, 14%) were collected in carboys
on 28/02/2019 from the Bras del Port solar saltern ponds: Sal6 (38°11'52.30"N,
0°36'13.15"W), Sall4 (38°12'4.74"N, 0°35'43.14"W). Brine samples were taken to the
Alicante laboratory for immediate serial filtration (as above) and DNA purification.
185 Freshwater (10 l) from a shallow lake in North-western France (Etang des Vallées;
48°41'23,0''N, 01°54'59.2''E) [44] was collected on 18/03/2019. Filtration was immediately
carried out at the Orsay laboratory as above except we used filters of 100, 30, 5 and 0.22 µm
pore-size, to avoid the many suspended plant material-derived particles in this shallow lake)
In all cases, 4-ml aliquots of the different size-fraction filtrates and the final eluate (<50 kDa)
190 were taken for flow cytometry and fixed overnight at 4°C with 0.5% glutaraldehyde then
frozen in dry ice and stored at -80°C (Table S6). DNA from cellular fractions was purified
from filters. These were cut into small pieces with a scalpel, added to 5 ml CTAB lysis buffer
(SERVA) with 1 mg/ml lysozyme and incubated at 37°C for 1 h. After addition of proteinase
K (0.2 mg/ml) and vortexing, the mix was incubated at 55°C for one additional hour prior to
195 phenol/chloroform/isoamyl alcohol (25:24:1, pH 8) and chloroform/isoamyl alcohol
extraction. Nucleic acids were precipitated overnight at -20°C with 1/10 volume of 3 M
sodium acetate, pH 5.2, and 2.5 volumes of absolute ethanol. After centrifugation at 4°C,
13000 x g for 30 min, the pellet was washed with 70% ethanol, centrifuged again and speed-
vac dried before resuspension in 10 mM Tris-HCl, pH 8.0. To purify DNA from viral
200 concentrates, we incubated them with 20 mM EDTA, 50 ng/µl proteinase K and 0.2% SDS
(final concentrations) for 1 h at 55°C and proceeded with the phenol/chloroform extraction as
before. To recover the maximum of the aqueous phase, we used MaXtract High Density
(Qiagen). DNA from the different cell fractions was fluorometrically quantified using Qubit
and mixed proportionally according to the same amount of original water sample as indicated
205 in Table S7. For all samples, we prepared a DNA mix "all" which included DNA from the
viral and all cellular fractions below 200 µm (100 µm for EdV) and a mix "0.2v" which
contained DNA from viral particles and cells smaller than 5 µm (prokaryotes and small
protists). All these mixes were used for metagenome sequencing. As an internal control for
our fractionation process, we also sequenced DNA from the viral fraction (metaviromes)
210 from the Mediterranean plankton (Table S8).

Flow cytometry

We quantified virus-like particles (VLP) and cells (up to ~10 μm) by flow cytometry (FCM) in the glutaraldehyde-fixed samples spanning different salinities and size fractions described above (Table S6). We used a CytoFLEX S (Beckman Coulter) equipped with two active diode lasers (488 nm and 561 nm) following well-established protocols [45, 46]. The flow cytometer settings and gains were, for VLP detection, forward scatter (FSC) 500, side scatter (SSC) 500 and green fluorescence (FITC) 400 with a threshold set to FITC 260; and, for cell detection, FSC 250, SSC 700 and FITC 70 with a threshold set to FITC 1000. The sheath fluid consisted of 0.1 μm -filtered Milli-Q water. Multifluorescent beads of 0.2 and 1 μm (Polyscience) were used as size reference for VLP and cells. Samples were thawed on ice and diluted up to 1000 times for VLP counts and 10 times for cell counts with 0.02 μm -filtered autoclaved Milli-Q water, TE buffer (Sigma) or seawater. VLP and cells were stained with SYBRGreen I (Sigma) for 10 min in the dark at 80°C and let cool down for 5 min at room temperature [46]. Background noise was systematically checked on blanks (Fig. S2). Samples were recorded with an event rate per second of 100-1,000 (VLP) and <300 (cells). For VLP, we defined three gates (V1, V2, V3) on a FITC-A vs SSC-A plot (Fig. S2). The VLP signal intensity was determined on marine plankton controls, with gates set to exclude background based on FITC signal. Cells were stained with SYBRGreen I for 10 min at room temperature in the dark. For cell counts, we established two gates, HDNA and LDNA, on a FITC-A vs SSC-A plot, as previously described [45]. Sample counts were analysed with CytExpert and Kaluza softwares (Beckman Coulter). VLP and cell counts were obtained by correcting the measured total counts for noise (typically having the lowest green fluorescence) using blanks. VLP and cell abundances were respectively expressed as VLP. ml^{-1} or Cells. ml^{-1} (Table S6).

235

DNA purification of sediment and microbial mats, sequencing and selection of natural metagenomes

We also included in this analysis metagenomes of freshwater sediments and microbial mats from previous and ongoing studies in our laboratory (Table S8). DNA from Lake Baikal sediment samples collected in July 2017 was purified using the Power Soil DNA purification kit (Qiagen, Germany) [47]. DNA from microbial mat samples collected from the Salada de Chiprana (Spain, December 2013), lakes Bezymyanoe and Reid (Antarctica, January 2017) and several hot springs around Lake Baikal (Southern Siberia, July 2017), fixed *in situ* in ethanol as previously described [48], was purified using the Power Biofilm DNA purification kit (Qiagen, Germany). DNA was quantified using Qubit. Sequencing (Illumina HiSeq, paired-end, 2x125 bp) was performed by Eurofins Genomics (Ebersberg, Germany). In total,

245

we generated 12 metagenomes from planktonic fractions coming from increasingly saline waters (freshwater, marine and solar saltern ponds at 6-14% salt), 8 metagenomes from freshwater sediment and 23 metagenomes of diverse microbial mats. To these, we added 13
250 metagenomes of other microbial mats and 7 from microbialites (18 of which were previously generated in our laboratory), 26 metagenomes from lake sediments, 6 marine sediment metagenomes, 16 soil metagenomes and 30 animal-associated microbiomes from diverse organs and animals (honey bees, frogs, humans), all of which were sequenced with the same technique (Illumina). In total, we included 133 metagenomes in this study (2 of them were
255 control Mediterranean metaviromes), 40 metagenomes generated in our laboratory and 93 metagenomes from other published studies [48-61] (an extended description, GenBank accession numbers and statistics are provided in Table S8).

Sequence analysis, annotation and taxonomic assignation of natural metagenomes

260 We treated the 133 metagenomic datasets with exactly the same bioinformatics pipeline starting from raw Illumina sequences. Read quality was verified with FastQC [62] v0.11.8 and cleaned with Trimmomatic [63] v0.39, adjusting the parameters as needed (usually LEADING:3 TRAILING:3 MAXINFO:30:0.8 MINLEN:36) and eliminating the Illumina adapters if any. Clean reads were assembled with Metaspades [40] v3.13.1 with default
265 parameters and k-mer iteration cycles of “21,25,31,35,41,45,51,55”. A few complex metagenomes that failed to assemble in our server were assembled with Megahit [64] v1.2.6 with default parameters except for a minimum contig length of 200 bp and starting kmer sizes of 23 to 93 with an increasing step of 10 (Table S8). Gene annotation was performed with Prokka [41] v1.14.5 in metagenome mode (contigs >200 bp). We assigned coding sequences
270 to PFAMs (Pfam-A database v3.1b2) with HMMER hmmsearch [27] v3.2.1 with the trust cut-off threshold. As PhiX174 genomic DNA is sometimes added during sequencing as internal control, we downloaded the reference phage PhiX174 genome and BLASTed the 11 encoded proteins against the set of significant MCPs of each metagenome. Hits to PhiX174’s MCP (NP_040711.1) with 100% identity over a 90% coverage were excluded from the
275 analysis. Taxonomy was assigned to each gene in metagenomes as described above for the mock metagenomes. Taxon-assigned genes were then classified using an *ad hoc* Perl script (assignTaxa.pl) into the following major groups, further classified in three major lifestyle categories: i) CPR bacteria (Patescibacteria) and DPANN archaea (Table S9), considered as cellular episymbionts/parasites strictly dependent on free-living organisms; ii) ”Other
280 Archaea”, ”Other Bacteria” and “Eukaryotes”, classed as free-living (FL), and iii) viruses. An

ad hoc Perl script (tax2PFAM.pl) linked each gene's taxonomy to its Pfam assignment. Metagenome-inferred proteins with >35% amino acid identity over >70% sequence length to viral genome-encoded proteins were assigned to the respective family, host and virus group. Viral taxonomy and Baltimore classification were determined with the VPF-Class tool [65] (Table S10). MCP-containing contigs were used as an input for VPF-Class; we attributed a classification when values were over a membership ratio score of 0.75. The relative abundance of MCPs from these contigs in metagenomes were plotted using the R ggplot2 package visualizing the different viral families and Baltimore classification.

290 **Diversity indices**

To calculate diversity estimates, we selected the most abundant USCG per group of metagenome (Table S11). Amino acid sequences for each ribosomal protein were retrieved with *ad hoc* Perl scripts for each metagenome group and clustered with cd-hit [66] at 99% identity (parameters -c 0.99, -n 5, -d 0, -T 16, -M 0). These clusters were considered operational taxonomic units (OTUs) and were assigned to CPR, DPANN, (non-DPANN) archaea, (non-CPR) bacteria and eukaryotes. For viruses, we used the whole set of viral MCPs under the premise that most viral genomes have only one MCP (see above). We obtained a total of 8,610 cellular clusters and 28,319 MCP clusters using Prokka annotation. Abundance matrices of these clusters were built with an *ad hoc* Perl script and several diversity indices (alpha diversity, Shannon entropy, Pielou's evenness and Simpson's dominance) were calculated with an *ad hoc* R script using the Vegan package [67]. Indices for all metagenomes were plotted with ggplot2. To compare if the difference between the viral and cellular diversity was significant, a Wilcoxon test was applied to the median of the alpha diversity per ecosystem, using an *ad hoc* R script with the ggpubr library. Visualization of the statistical test was represented as a box plot with the same R script and the ggplot2 library. Principal component analyses (PCA) of different diversity indices as a function of metagenomes were carried out with an *ad hoc* R script, and visualized using the ggplot2 package.

310 **Results**

Benchmarking mVMR in mock metagenomes

To develop a metagenome-based VMR estimate, we used universal single-copy genes (USCGs) and viral major capsid protein (MCP) genes, usually present in single copy in viral

genomes, as proxies for cells and DNA viruses, respectively. We selected 15 ribosomal
315 proteins that are well-represented across the three domains of life as USCGs (Table S1). To
limit differential representation of individual ribosomal protein genes, we averaged values for
the 15 USCGs as a proxy for cell counts under the assumption that in most biomes cells
contain one genome copy. Relatively rare cases of polyploidy have been described, e.g. in
320 giant bacteria [68, 69] and haloarchaea [70], and two chromosome copies usually occur in
some archaea and actively transcribing bacteria [71]. However, in the wild, especially in
energy-limited ecosystems, microbial cells are likely to exist in low average metabolic states
and, consequently, limited ploidy. Should average ploidy be higher than one, this proxy
might slightly overestimate cell numbers. Conversely, some markers do not capture well
325 episyntrophic prokaryotes with reduced and divergent genomes, such as Candidate Phyla
Radiation (CPR or Patescibacteria) bacteria and DPANN archaea [72, 73], which might
partly compensate for the ploidy excess in some cells. To count viruses, we used 132 hidden
Markov models (HMMs) that recognize MCPs from virtually all known families of DNA
viruses infecting bacteria, archaea and eukaryotes. In addition, to avoid missing MCPs from
potential unknown viruses present in the studied natural metagenomes (see below), we
330 designed specific HMMs for viral genomes assembled from them (Table S2; see Methods).
We then generated 10 mock metagenomes with increasing VMRs, ranging from ratios of 10
cells per viral genome (V001M10; the number following V and M indicates the ratio of viral
to microbial cell genomes per mock metagenome) to 125 viral genomes per microbial cell
(V125M01). We also included one metagenome with only cellular genomes (V000M01) and
335 one with only viral genomes, i.e. a metavirome (V001M00). These mock metagenomes partly
mimicked marine planktonic communities, and included genomes of archaea, bacteria,
eukaryotes and viruses (Table S3).

The assemblies in the mock metagenomes with the highest VMR (V042M01 and
V125M01) were highly fragmented, exhibiting lower quality (Fig. 1A; Table S4). To cope
340 with potential gene detection problems in these assemblies, we applied two annotation
strategies, one based on predicted gene annotation (Prokka [41]) and another based on the
annotation of all possible open reading frames (OrfM [42]) allowing for the detection of
individual protein domains even if genes were fragmented. Even if many more ORFs than
genes were detected per mock metagenome (Fig. S1A), the amounts and relative proportions
345 of USCGs per metagenome were remarkably similar between the two methods except for
those with the highest VMR, where OrfM performed quantitatively better (Fig. S1B). The
relative proportions of high-rank cellular taxa obtained with the two annotation strategies

were closely similar (Fig. S1C-D) and in agreement with the expected taxonomic assignment (Table S5). To estimate mVMR, we searched for USCGs and MCPs in the assembled contigs from these 10 metagenomes using the respective protein family HMMs (see Methods) and, after mapping the original reads onto the identified contigs, obtained normalised USCG and MCP numbers by counting the reads per kilobase of gene sequence per million of mapped metagenome reads (RPKMs). The inferred mVMR values were also similar for the two annotation strategies, and close to the expected VMR although, at very high VMR (V125M001), OrfM yielded slightly lower mVMR values than Prokka (Fig.1B). As expected, we could not detect USCGs in genes/ORFs predicted from the virus-only mock metavirome (V001M00). However, we did identify several MCPs in the metagenome containing only cellular genomes (V000M001). These were annotated as cellular virus-related or hypothetical proteins/domains by Prokka and corresponded to proviruses present in the included cellular genomes (Table S3). Accordingly, it was possible to differentiate lysogenic viruses from VPs and intracellular lytic viruses in these mock metagenomes (Fig.1C; Fig. S1C-D). The presence of proviruses likely explains the observation that, at very low VMR (V000M001-V001M10), viral counts appeared slightly overestimated (Fig.1C).

365 **Estimation of mVMR in aquatic metagenomes**

After benchmarking mVMR in mock metagenomes, we first sought to estimate mVMRs for aquatic ecosystems and compare the resulting values to classical epifluorescence-derived estimates (fVMR). However, published planktonic metagenomes are not suitable for the estimation of total mVMRs due to an inherent problem resulting from the fact that DNA is purified from the planktonic biomass retained on different pore-size filters upon filtration. Most of the available aquatic metagenomes contain the prokaryotic/picoeukaryotic fraction (0.2 to 3-5 μm cell size) and, more rarely, larger-size fractions where many protists are retained (>5 and up to 100-200 μm). Metagenomes from smaller plankton fractions containing VPs (“metaviromes”) are obtained after tangential filtration of <0.2 μm filtrates to retain particles larger than 50-100 kDa. However, many VPs can be also retained in pre-filtration steps and end up in “cellular” fractions, for instance retained on membranes in-between pores and, especially, trapped among cells as filters saturate with biomass. A corollary is that cellular metagenomes and metaviromes are usually generated from different water volumes/samples, after imperfect particle fractionation steps, sequenced from different libraries and analysed separately, such that mVMR cannot be directly and reliably estimated. To overcome this problem, we generated integral microbial plankton metagenomes, including

genomes of both cells and viruses (covering both extracellular and intracellular phases of the virus replication cycle), from the same water mass of selected aquatic ecosystems (Fig. 2). They included a freshwater shallow lake in Northern France (Etang des Vallées, EdV), the
385 Western Mediterranean water column (sampled at 20 and 40 m depth) and two ponds of increasing salinity (6% and 14% salt) from a Mediterranean solar saltern (Table S8). To obtain more representative VMR, we sampled these ecosystems in late winter (see Methods), avoiding massive blooming periods when richness and evenness decrease [74].

To generate metagenomes of coexisting viral and microbial cell plankton, we carried out
390 serial filtration steps from the same initial water mass through filters of 200 μm pore-diameter to exclude metazoans larger than that size and then 20, 5 and 0.2 μm , retaining cells of different sizes. Tangential filtration was applied to the resulting $<0.2 \mu\text{m}$ -filtrate to concentrate viral particles ($>50 \text{ kDa}$) (Fig. 2). We retained aliquots of all sequential filtrates for fluorescent cytometry (FCM) counts of labelled cells and VLPs, and the final eluate (<50
395 kDa) as a blank (Table S6 and Fig. S2). FCM counts of cells in all fractions $>0.2 \mu\text{m}$ were consistently similar for each sample type, indicating that the vast majority of cells were prokaryotic. Cell abundances were higher in saltern ponds (5.2×10^6 to $1.0 \times 10^7 \text{ cells.ml}^{-1}$) and freshwater samples (4.3 to $4.7 \times 10^6 \text{ cells.ml}^{-1}$) compared to marine samples, for which the counts were about an order of magnitude lower (4.5 to $\times 10^5 \text{ cells.ml}^{-1}$) (Fig. 3A; Table S6).
400 VLP counts were also consistent in large-size fractions of each sample and diminished in the tangential-filtration concentrate. This observation indicates that many VLPs were retained in larger fractions due to progressive filter saturation with biomass and highlights the importance of combining different size fractions of the same filtration series for metagenome-based abundance estimates. VLP abundances appeared higher in saline environments
405 (5.6×10^7 and $4.1 \times 10^7 \text{ VLP.ml}^{-1}$ for 6% and 14% salt ponds, respectively). Although this could reflect the actual abundance of viruses, it is also possible that salt nanoprecipitates forming at increasing salinities get unspecifically fluorescently stained [18]. Estimated fVMRs ranged from ~ 3 to 15, with lower values for freshwater (~ 4), 40 m-deep Mediterranean (~ 5) and 14%-salt pond (~ 3) and higher for 20 m-deep Mediterranean (~ 14) and 6% (~ 10) saltern
410 ponds (Fig.3A and D; Table S6).

We purified DNA from the biomass retained on all filters used during serial filtration as well as from tangential-filtration concentrates, keeping track of the corresponding water volumes. DNA samples obtained from different fractions were then proportionally mixed for a given original water volume (Table S7). We sequenced metagenomes from two plankton
415 fractions including viral particles and cells up to i) 5 μm , i.e. prokaryotes and pico-

nanoeukaryotes (50 kDa - 5 μ m; "02v" fraction), and ii) 200 μ m (100 μ m for EdV), including unicellular prokaryotes and pico-nano-microeukaryotes (50 kDa - 200 μ m; "all" fraction) (Fig. 2). In this way, co-occurring viral and cellular DNA was sequenced from the same library, avoiding technical biases. As eukaryotes represented a minor fraction in these aquatic systems, the two metagenomes were expected to behave as quasi-replicates for mVMR
420 inference. In addition, we sequenced two "metavirome" fractions (50 kDa - 0.2 μ m; "vir" fraction) for the marine samples as internal controls (Table S8). Normalised numbers of USCGs were generally congruent in our aquatic metagenomes, although with slight among-marker differences (Fig. S3). In all our planktonic metagenomes, normalised viral counts
425 (MCPs) were higher than USCG-based cell counts (Fig. 3B). Most cell counts were bacterial; as expected, eukaryotic counts were comparatively low (Fig. 3B).

Estimates of mVMR in our aquatic ecosystems varied between 1.3 and 10.5, with marine samples exhibiting values of 3-4 (Fig. 3C-D; Table S8). mVMRs were lower than fVMR in marine and saline samples (Fig. 3D), although the two values were comparable in the case of
430 MedD (~4-6) and Sall4 (~2-3). By contrast, in the case of freshwater EdV samples, mVMR values were 3 times higher than fVMRs. This difference seems to suggest that, in addition to VPs, intracellular lytic viruses and/or proviruses were highly prevalent in the plankton of this highly diverse shallow lake [75].

435 **mVMR across ecosystems**

We subsequently calculated mVMRs in additional metagenomes (for a total of 131, leaving aside the two metaviromes; Table S8) covering a wide biome diversity including marine and lake sediments, soils, microbial mats growing in various conditions (halophilic to thermophilic), microbialites and several types of metazoan-associated microbiomes. Many of
440 those metagenomes were retrieved from public databases but 40 of them were generated in our laboratory, notably from poorly studied ecosystems (Table S8). To avoid potential confounding factors derived from sequencing techniques and bioinformatic analysis, all chosen metagenomes were sequenced using the same technology and treated uniformly starting from raw reads. Although normalised viral MCPs tended to dominate over cellular
445 USCGs across the 131 studied metagenomes, cellular markers dominated in about a third of them and, in several metagenomes, viral and cellular counts were comparable (Fig. 4; Fig. S4-S5).

At finer taxonomic scales, the diversity and relative proportions of cellular organisms and viruses were overall congruent with those reported for the different types of ecosystems

450 and the specific studied metagenomes (Table S8). Bacterial taxa were largely dominant across biomes, although archaea and microbial eukaryotes were also present (Fig. 5A; Fig. S5). Archaea were abundant in marine sediments [49], several microbial mats [48] and the surface Mediterranean waters, the latter dominated by Marine Group II archaea (Fig. 5A). Diverse Alpha- and Gammaproteobacteria were highly abundant in marine plankton but also
455 in microbialites and, to a lesser extent, microbial mats. Cyanobacteria were also present in considerable proportions in these ecosystems. Actinobacteria and Acidobacteria were dominant in soils. Some actinobacterial taxa were also abundant in the freshwater system [75]. Microbial eukaryotes consistently occurred in most ecosystems, albeit in minor proportions. They were more abundant in plankton samples and microbialites; diverse
460 microalgae, notably diatoms and chlorophytes dominated the eukaryotic component (Fig. 5A). The abundances of CPR and DPANN (the latter included in “other archaea” in Fig. 5A) were generally relatively low (albeit reaching ~10% in some samples) and did not outnumber viruses in the same ecosystems, suggesting that viral parasitism is generally more prevalent than prokaryotic parasitism.

465 Viruses were also highly diverse although, as expected, dsDNA viruses largely dominated the studied microbial ecosystems; ssDNA viruses were also detected (Fig. S6; Table S10). In agreement with the pronounced dominance of bacteria as potential hosts in most biomes, the dominant identified viral families belonged to the class *Caudoviricetes* (tailed bacteriophages and related archaeal viruses [76], containing the HK97-fold MCP),
470 which collectively represent ~74% (n=8281) of all identified viral contigs across ecosystems. The bacteriophage family *Microviridae*, with ssDNA genomes, was represented in some ecosystems. Among eukaryotic viruses, the most represented were members of the *Phycodnaviridae*, which typically parasitize algae, and *Mimiviridae*, which infect diverse protists (e.g. amoeba) [77] (Fig. 5B; Table S10).

475 In summary, although the inferred mVMR values were on average greater than 1 (global average 1.96, i.e. ~2 viruses per cell), mVMR values were lower than 1 in approximately one third of the metagenomes (Fig. 4). In only 5 out of the 131 metagenomes, viruses exceeded cells by more than one order of magnitude. The rest of the metagenomes displayed mVMR values between 1 and ~7. In terms of grand ecosystem types, mVMR were the highest in
480 aquatic ecosystems (mean 4.0; median 3.0) and the lowest in animal-associated microbiomes (mean 1.3; median 0.8; Fig. 6A), consistent with the low recent VMR estimates in the human gut [78]. Microbial mats and soils/sediments exhibited intermediate average values

(respective means, 1.5 and 3.1, and medians, 1.1, 1.0), the latter displaying a wider value distribution with a higher variance, in agreement with previous observations [19-21].

485 To look for potential determinants explaining the distribution of viruses and cells across biomes, we carried out principal component analyses (PCA) of the studied metagenomes using diversity-related parameters, namely richness, alpha-diversity and evenness indices for cells and viruses (Fig. S7). As expected, cell alpha-diversity positively correlated with microbial mats and soils, being lower in host-related microbiomes, whereas viral diversity
490 best correlated with marine and freshwater plankton. Cell evenness mostly correlated with some soil and microbialite samples, whereas viral evenness correlated with freshwater sediment samples (Fig. 6 for grand ecosystem types; Fig. S8 for more detailed ecosystems). Globally, alpha-diversity values estimated for cells and viruses were significantly different among specific (Fig. S8B) and grand ecosystem (Fig. 6B) types. The alpha-diversity of viral
495 plankton was the highest followed, albeit at a distance, by sediments, both freshwater and marine (Fig. 6B; Fig. S8B). This trend, along with higher viral abundances, is consistent with the notion that water masses constitute a reservoir of dispersing viral particles. By contrast, highly structured and heterogeneous environments are less prone to host a wide and abundant diversity of dispersing forms because, in the absence of their specific hosts, these particles
500 can be easily used as food or otherwise degrade. Freshwater and marine sediments would appear as intermediates, receiving a constant input of sedimenting VPs, which can then enter a decay and degradation process associated to local prokaryotic communities.

Discussion

505 In this work, we developed and benchmarked on mock metagenome datasets a metagenome-based VMR metric based on virus and cell markers that is applicable throughout microbial ecosystems in a comparative manner. Our mVMR metric is *a priori* more accurate for the inference of actual (DNA) virus:microbe ratios because, in comparison with fVMR values based on fluorescently labelled VLPs only, it accounts also for the actively infecting,
510 intracellular lytic viruses as well as lysogenic forms. Our approach is thus more viral-inclusive and free from potential biases affecting fVMR [10, 12-14, 16-18]. In addition to identifying specifically stained vesicles and capsids containing non-viral DNA (transducing phages or gene transfer agents), fluorescence-based methods are affected by biases stemming from the differential treatment of contrasting sample types (water, soil, sediment,
515 mucilaginous mats) and can include non-specifically stained organic and/or mineral particles

from complex ecosystems. These artefacts may not only affect VLP counts, but possibly also cell counts, casting doubt on total cell estimates based on these methods in sediments, soils or the subsurface and, hence, global virus and cell counts [9, 10]. Furthermore, because a sizable fraction of viral particles is defective [79-81], the real number of infective viruses derived from VLP counts remains uncertain.

Our approach is not fully devoid of potential biases that might result in slight relative over- or underestimates of cells and/or viruses, such as differences in cell ploidy or divergent viral and cellular individual gene markers. However, as metagenome sequencing and the exploration of cellular and viral diversity across ecosystem types improve, detection problems linked to sequence divergence should be gradually solved. Obviously, being metagenome-based, our approach does not allow for the quantification of RNA viruses and, for reverse-transcribing viruses and single-stranded DNA viruses, only the replicative DNA intermediates can be identified. Notably, epifluorescence-based approaches are equally unsuited for enumeration of viruses with small RNA and ssDNA genomes due to lack of sensitivity [82]. Thus, the numbers of their virus particles will be slightly underestimated using both the metagenomic approach described herein and the traditional fluorescence-based counting. Unfortunately, a similar approach based on metatranscriptomic counts is not feasible to infer VMRs for RNA viruses because USCGs can be expressed at drastically different levels in different cells, preventing them to be used as markers for individuals. Like DNA viromes uncovered by metagenomic studies [7, 83], the diversity of the global RNA virome is rapidly expanding thanks to metatranscriptomic analyses [84-86]. Nonetheless, dsDNA viruses dominate the prokaryotic virome [77] and, although several novel families of RNA viruses seem to infect bacteria [84, 85], bacterial viruses jointly comprise only 3.4% of the RNA viral OTUs [84]. Therefore, given that most microbial ecosystems are overwhelmingly dominated by prokaryotes, mVMR estimates based on gene-marker proxies for individual viruses and cells, even if in need of further refinement (especially with progressively expanding databases), are likely to be the best current approximation of the real VMR, at least at the order-of-magnitude level.

This work shows that mVMRs are higher in planktonic systems approaching, albeit not necessarily reaching, the values of ~10:1 that are traditionally assumed to be the minimal values in current (fVMR-based) estimates (Fig. 6). Water masses therefore seem to represent reservoirs of viral particles that can more easily escape from cellular predation, whereby nucleic acids serve as an excellent source of P and N, even if the uptake of specific lytic viral nucleic acids comes at a cost [87]. From this perspective, aerosols likely are another huge

550 reservoir of VPs. By contrast, in higher-density biomes, mVMR values appear substantially
lower, consistent with higher viral dispersal limitation and degradation rates, as well as with
the idea that VMR declines as a function of microbial cell densities [23]. Even if mVMRs are
highly variable, especially in sediments and soils, mVMR estimates across non-aquatic
ecosystems barely reach 2, being especially low in cell-dense multicellular host-associated
555 microbiomes (<1). Overall, our mVMR estimates across ecosystems question the currently
widely held assumption that viruses outnumber cells at least by one order of magnitude. Even
if ocean waters occupy an important fraction of Earth's volume, continental biomes together
with the deep subsurface undoubtedly host most of the planet's biomass and cells [88, 89].
Accordingly, although viruses likely are the most diverse biological entities on Earth [6, 7],
560 notably because most cellular organisms can be infected by different viruses, they might
quantitatively be almost at equal footing with cells. In addition, deciphering the proportion of
actively infecting viruses should provide more useful information about the maximum load of
viral entities that microbial communities can support before ecosystems collapse. Future
exploration of these poorly studied parameters across ecosystems and along temporal series
565 should help understanding the dynamics of viral-cell interactions in the biosphere.

Acknowledgements

We thank José Manuel Haro Moreno for help during marine and solar saltern sampling in
Alicante, Paola Bertolino for help during sampling in several other ecosystems, and Antonio
570 Camacho y Antonio Picazo for CTD measurements during marine plankton sampling. We
thank the Salinas Bras del Port for sampling permission and the UNICELL platform for flow
cytometry analyses. We acknowledge support from the Moore-Simons Project on the Origin
of the Eukaryotic Cell through Grant GBMF9739 (P.L.-G.) and the European Research
Council Advanced Grants FP7 No. 322669 (P.L.-G.) and H2020 No. 787904 (D.M.).

575

Competing interests. The authors declare no competing interests.

Data and code availability

Metagenome Illumina sequences generated in our laboratory and not yet published have been
580 deposited in GenBank (National Center for Biotechnology Information) Short Read Archive
with BioProject number PRJNA756245. Accession numbers for all used metagenomes are
provided in Table S8. Metagenome assemblies generated for this study are available here:
<https://www.deemteam.fr/en/datasets>. The corresponding proteomes as well as the HMM

profiles are available in FigShare (<https://figshare.com/projects/mVMRs/159701>) and all
585 code is available in GitLab (<https://gitlab.com/anagtz/mvmrs>).

Author contributions. P.L.-G. and D.M. conceived the study and designed experiments, organized and participated in sampling and successive filtration steps, did the tangential filtration and quantitatively purified DNA from the different cell and viral fractions. A.G.-P. participated in sampling and carried out all bioinformatic analyses, with informatics support by P.D. M.K. designed the HMM profiles for MCPs. M.C. carried out flow cytometry counts of viruses and cells with the assistance of L.J. M.L.-P. and F.R.-V. co-organized sampling in marine and solar saltern sites and helped with filtration on board. P.L.-G. wrote the manuscript with input from A.G.-P. and M.C. All authors read, commented and approved the
595 manuscript.

References

1. Fuhrman JA. Marine viruses and their biogeochemical and ecological effects. *Nature*. 1999; 399: 541-548.
- 600 2. Suttle CA. Marine viruses--major players in the global ecosystem. *Nat Rev Microbiol*. 2007; 5: 801-812.
3. Thingstad TF. Elements of a theory for the mechanisms controlling abundance, diversity, and biogeochemical role of lytic bacterial viruses in aquatic systems. *Limnol Oceanogr*. 2000; 45: 1320-1328.
- 605 4. Rodriguez-Valera F, Martin-Cuadrado AB, Rodriguez-Brito B, Pasic L, Thingstad TF, Rohwer F *et al*. Explaining microbial population genomics through phage predation. *Nat Rev Microbiol*. 2009; 7: 828-836.
5. Rohwer F, Thurber RV. Viruses manipulate the marine environment. *Nature*. 2009; 459: 207-212.
- 610 6. Paez-Espino D, Zhou J, Roux S, Nayfach S, Pavlopoulos GA, Schulz F *et al*. Diversity, evolution, and classification of virophages uncovered through global metagenomics. *Microbiome*. 2019; 7: 157.
7. Dion MB, Oechslin F, Moineau S. Phage diversity, genomics and phylogeny. *Nat Rev Microbiol*. 2020; 18: 125-138.
- 615 8. Bergh O, Børsheim KY, Bratbak G, Heldal M. High abundance of viruses found in aquatic environments. *Nature*. 1989; 340: 467-468.
9. Cobián Güemes AG, Youle M, Cantú VA, Felts B, Nulton J, Rohwer F. Viruses as winners in the game of life. *Annu Rev Virol*. 2016; 3: 197-214.
10. Mushegian AR. Are there 10^{31} virus particles on Earth, or more, or less? *J Bacteriol*. 2020; JB.00052-00020.
- 620 11. Suttle CA. Viruses in the sea. *Nature*. 2005; 437: 356-361.
12. Forterre P, Soler N, Krupovic M, Marguet E, Ackermann HW. Fake virus particles generated by fluorescence microscopy. *Trends Microbiol*. 2013; 21: 1-5.
- 625 13. Schatz D, Rosenwasser S, Malitsky S, Wolf SG, Feldmesser E, Vardi A. Communication via extracellular vesicles enhances viral infection of a cosmopolitan alga. *Nat Microbiol*. 2017; 2: 1485-1492.

14. Toyofuku M, Nomura N, Eberl L. Types and origins of bacterial membrane vesicles. *Nat Rev Microbiol.* 2019; 17: 13-24.
- 630 15. Liu J, Cvirkaite-Krupovic V, Commere PH, Yang Y, Zhou F, Forterre P *et al.* Archaeal extracellular vesicles are produced in an ESCRT-dependent manner and promote gene transfer and nutrient cycling in extreme environments. *ISME J.* 2021; 15: 2892-2905.
16. Lang AS, Westbye AB, Beatty JT. The distribution, evolution, and roles of gene transfer agents in prokaryotic genetic exchange. *Annu Rev Virol.* 2017; 4: 87-104.
- 635 17. Klauth P, Wilhelm R, Klumpp E, Poschen L, Groeneweg J. Enumeration of soil bacteria with the green fluorescent nucleic acid dye Sytox green in the presence of soil particles. *J Microbiol Methods.* 2004; 59: 189-198.
18. Belilla J, Iniesto M, Moreira D, Benzerara K, Gérard E, López-García JM *et al.* Active Microbial airborne dispersal and biomorphs as confounding factors for life detection in the cell-degrading brines of the polyextreme Dallol geothermal field. *mBio.* 2022; 13: e0030722.
- 640 19. Parikka KJ, Le Romancer M, Wauters N, Jacquet S. Deciphering the virus-to-prokaryote ratio (VPR): insights into virus-host relationships in a variety of ecosystems. *Biol Rev Camb Philos Soc.* 2017; 92: 1081-1100.
- 645 20. Danovaro R, Corinaldesi C, Filippini M, Fischer UR, Gessner MO, Jacquet S *et al.* Viriobenthos in freshwater and marine sediments: a review. *Freshw Biol.* 2008; 53: 1186-1213.
21. Williamson KE, Fuhrmann JJ, Wommack KE, Radosevich M. Viruses in soil ecosystems: an unknown quantity within an unexplored territory. *Annu Rev Virol.* 2017; 4: 201-219.
- 650 22. Wei M, Xu K. New insights into the virus-to-prokaryote ratio (VPR) in marine sediments. *Front Microbiol.* 2020; 11: 1102.
23. Wigington CH, Sonderegger D, Brussaard CPD, Buchan A, Finke JF, Fuhrman JA *et al.* Re-examination of the relationship between marine virus and microbial cell abundances. *Nat Microbiol.* 2016; 1: 15024.
- 655 24. Knowles B, Silveira CB, Bailey BA, Barott K, Cantu VA, Cobián-Güemes AG *et al.* Lytic to temperate switching of viral communities. *Nature.* 2016; 531: 466-470.
25. Weitz JS, Beckett SJ, Brum JR, Cael BB, Dushoff J. Lysis, lysogeny and virus-microbe ratios. *Nature.* 2017; 549: E1-E3.
- 660 26. Finn RD, Coggill P, Eberhardt RY, Eddy SR, Mistry J, Mitchell AL *et al.* The Pfam protein families database: towards a more sustainable future. *Nucleic Acids Res.* 2016; 44: D279-285.
27. Potter SC, Luciani A, Eddy SR, Park Y, Lopez R, Finn RD. HMMER web server: 2018 update. *Nucleic Acids Res.* 2018; 46: W200-w204.
28. Buchfink B, Xie C, Huson DH. Fast and sensitive protein alignment using DIAMOND. *Nat Methods.* 2015; 12: 59-60.
- 665 29. Menzel P, Ng KL, Krogh A. Fast and sensitive taxonomic classification for metagenomics with Kaiju. *Nat Commun.* 2016; 7: 11257.
30. de Miranda Boratto PV, Oliveira GP, Abrahão JS. "Yaraviridae": a proposed new family of viruses infecting *Acanthamoeba castellanii*. *Archiv Virol.* 2022; 167: 711-715.
- 670 31. Kauffman KM, Hussain FA, Yang J, Arevalo P, Brown JM, Chang WK *et al.* A major lineage of non-tailed dsDNA viruses as unrecognized killers of marine bacteria. *Nature.* 2018; 554: 118-122.
32. 2. Gaïa M, Meng L, Pelletier E, Forterre P, Vanni C, Fernandez-Guerra A *et al.* Mirusviruses link herpesviruses to giant viruses. *Nature.* 2023. In press. doi: 10.1038/s41586-023-05962-4.
- 675 33. Remmert M, Biegert A, Hauser A, Söding J. HHblits: lightning-fast iterative protein sequence searching by HMM-HMM alignment. *Nat Methods.* 2011; 9: 173-175.

34. Steinegger M, Meier M, Mirdita M, Vöhringer H, Haunsberger SJ, Söding J. HH-suite3 for fast remote homology detection and deep protein annotation. *BMC Bioinformatics*. 2019; 20: 473.
- 680 35. Mistry J, Finn RD, Eddy SR, Bateman A, Punta M. Challenges in homology search: HMMER3 and convergent evolution of coiled-coil regions. *Nucleic Acids Res*. 2013; 41: e121.
36. Langmead B, Salzberg SL. Fast gapped-read alignment with Bowtie 2. *Nat Methods*. 2012; 9: 357-359.
- 685 37. Li H, Handsaker B, Wysoker A, Fennell T, Ruan J, Homer N *et al*. The sequence alignment/map format and SAMtools. *Bioinformatics*. 2009; 25: 2078-2079.
38. Wickham H. *ggplot2: Elegant Graphics for Data Analysis*. Springer-Verlag New York. 2016.
- 690 39. Mende DR, Waller AS, Sunagawa S, Järvelin AI, Chan MM, Arumugam M *et al*. Assessment of metagenomic assembly using simulated next generation sequencing data. *PLoS One*. 2012; 7: e31386.
40. Nurk S, Meleshko D, Korobeynikov A, Pevzner PA. metaSPAdes: a new versatile metagenomic assembler. *Genome Res*. 2017; 27: 824-834.
- 695 41. Seemann T. Prokka: rapid prokaryotic genome annotation. *Bioinformatics*. 2014; 30: 2068-2069.
42. Woodcroft BJ, Boyd JA, Tyson GW. OrfM: a fast open reading frame predictor for metagenomic data. *Bioinformatics*. 2016; 32: 2702-2703.
- 700 43. Ghai R, Martin-Cuadrado AB, Molto AG, Heredia IG, Cabrera R, Martin J *et al*. Metagenome of the Mediterranean deep chlorophyll maximum studied by direct and fosmid library 454 pyrosequencing. *ISME J*. 2010; 4: 1154-1166.
44. Simon M, Lopez-Garcia P, Deschamps P, Moreira D, Restoux G, Bertolino P *et al*. Marked seasonality and high spatial variability of protist communities in shallow freshwater systems. *ISME J*. 2015; 9: 1941-1953.
- 705 45. Gasol JM, del Giorgio PA. Using flow cytometry for counting natural planktonic bacteria and understanding the structure of planktonic bacterial communities. *Sci Mar*. 2000; 64: 197-224.
46. Wilhelm SW, Weinbauer MG, Suttle CA (eds): Quantification of aquatic viruses by flow cytometry. *Manual of Aquatic Viral Ecology*. *ASLO*.
- 710 47. Reboul G, Moreira D, Annenkova NV, Bertolino P, Vershinin KE, López-García P. Marine signature taxa and core microbial community stability along latitudinal and vertical gradients in sediments of the deepest freshwater lake. *ISME J*. 2021; 15: 3412-3417.
- 715 48. Gutierrez-Preciado A, Saghai A, Moreira D, Zivanovic Y, Deschamps P, Lopez-Garcia P. Functional shifts in microbial mats recapitulate early Earth metabolic transitions. *Nat Ecol Evol*. 2018; 2: 1700-1708.
49. Dong X, Greening C, Rattray JE, Chakraborty A, Chuvochina M, Mayumi D *et al*. Metabolic potential of uncultured bacteria and archaea associated with petroleum seepage in deep-sea sediments. *Nat Commun*. 2019; 10: 1816.
- 720 50. Dombrowski N, Teske AP, Baker BJ. Expansive microbial metabolic versatility and biodiversity in dynamic Guaymas Basin hydrothermal sediments. *Nat Commun*. 2018; 9: 4999.
51. Zhang X, Xu W, Liu Y, Cai M, Luo Z, Li M. Metagenomics reveals microbial diversity and metabolic potentials of seawater and surface sediment from a hadal biosphere at the Yap Trench. *Front Microbiol*. 2018; 9: 2402.

- 725 52. Ruuskanen MO, Colby G, St.Pierre KA, St.Louis VL, Aris-Brosou S, Poulain AJ. Microbial genomes retrieved from High Arctic lake sediments encode for adaptation to cold and oligotrophic environments. *Limnol Oceanogr.* 2020; 65: S233-S247.
53. Vavourakis CD, Mehrshad M, Balkema C, van Hall R, Andrei A-Ş, Ghai R *et al.* Metagenomes and metatranscriptomes shed new light on the microbial-mediated sulfur cycle in a Siberian soda lake. *BMC Biol.* 2019; 17: 69.
- 730 54. Ji M, Greening C, Vanwonderghem I, Carere CR, Bay SK, Steen JA *et al.* Atmospheric trace gases support primary production in Antarctic desert surface soil. *Nature.* 2017; 552: 400-403.
55. Xu J, Zhang Y, Zhang P, Trivedi P, Riera N, Wang Y *et al.* The structure and function of the global citrus rhizosphere microbiome. *Nat Commun.* 2018; 9: 4894.
- 735 56. Wilbanks EG, Jaekel U, Salman V, Humphrey PT, Eisen JA, Facciotti MT *et al.* Microscale sulfur cycling in the phototrophic pink berry consortia of the Sippewissett Salt Marsh. *Environ Microbiol.* 2014; 16: 3398-3415.
57. Saghai A, Zivanovic Y, Moreira D, Benzerara K, Bertolino P, Ragon M *et al.* Comparative metagenomics unveils functions and genome features of microbialite-associated communities along a depth gradient. *Environ Microbiol.* 2016; 18: 4990-5004.
- 740 58. Rebollar EA, Gutiérrez-Preciado A, Noecker C, Eng A, Hughey MC, Medina D *et al.* The skin microbiome of the neotropical frog *Craugastor fitzingeri*: Inferring potential bacterial-host-pathogen interactions from metagenomic data. *Front Microbiol.* 2018; 9.
- 745 59. Regan T, Barnett MW, Laetsch DR, Bush SJ, Wragg D, Budge GE *et al.* Characterisation of the British honey bee metagenome. *Nat Commun.* 2018; 9: 4995-4995.
60. Lloyd-Price J, Mahurkar A, Rahnavard G, Crabtree J, Orvis J, Hall AB *et al.* Strains, functions and dynamics in the expanded Human Microbiome Project. *Nature.* 2017; 550: 61-66.
- 750 61. Vangay P, Johnson AJ, Ward TL, Al-Ghalith GA, Shields-Cutler RR, Hillmann BM *et al.* US immigration westernizes the human gut microbiome. *Cell.* 2018; 175: 962-972.e910.
62. Wingett SW, Andrews S. FastQ Screen: A tool for multi-genome mapping and quality control. *F1000Res.* 2018; 7: 1338.
- 755 63. Bolger AM, Lohse M, Usadel B. Trimmomatic: a flexible trimmer for Illumina sequence data. *Bioinformatics.* 2014; 30: 2114-2120.
64. Li D, Luo R, Liu CM, Leung CM, Ting HF, Sadakane K *et al.* MEGAHIT v1.0: A fast and scalable metagenome assembler driven by advanced methodologies and community practices. *Methods.* 2016; 102: 3-11.
- 760 65. Pons JC, Paez-Espino D, Riera G, Ivanova N, Kyrpides NC, Llabrés M. VPF-Class: Taxonomic assignment and host prediction of uncultivated viruses based on viral protein families. *Bioinformatics.* 2021; 37: 1805-1813.
66. Fu L, Niu B, Zhu Z, Wu S, Li W. CD-HIT: accelerated for clustering the next-generation sequencing data. *Bioinformatics.* 2012; 28: 3150-3152.
- 765 67. Oksanen J, Blanchet G, Kindt R, Legendre P, O'Hara RB, Simpson GL *et al.* Vegan: Community Ecology Package. R package version 1.17-9. In: <http://CRAN.R-project.org/package=vegan> (ed). <http://CRAN.R-project.org/package=vegan>. 2011.
68. Mendell JE, Clements KD, Choat JH, Angert ER. Extreme polyploidy in a large bacterium. *Proc Natl Acad Sci U S A.* 2008; 105: 6730-6734.
- 770 69. Volland JM, Gonzalez-Rizzo S, Gros O, Tynl T, Ivanova N, Schulz F *et al.* A centimeter-long bacterium with DNA contained in metabolically active, membrane-bound organelles. *Science.* 2022; 376: 1453-1458.
70. Ludt K, Soppa J. Polyploidy in halophilic archaea: regulation, evolutionary advantages, and gene conversion. *Biochem Soc Trans.* 2019; 47: 933-944.

- 775 71. Touchon M, Rocha EP. Coevolution of the organization and structure of prokaryotic genomes. *Cold Spring Harb Perspect Biol.* 2016; 8: a018168.
72. Castelle CJ, Brown CT, Anantharaman K, Probst AJ, Huang RH, Banfield JF. Biosynthetic capacity, metabolic variety and unusual biology in the CPR and DPANN radiations. *Nat Rev Microbiol.* 2018; 16: 629-645.
- 780 73. Dombrowski N, Lee JH, Williams TA, Offire P, Spang A. Genomic diversity, lifestyles and evolutionary origins of DPANN archaea. *FEMS Microbiol Lett.* 2019; 366: fnz008.
74. Pommier T, Neal PR, Gasol JM, Coll M, Acinas SG, Pedrós-Alió C. Spatial patterns of bacterial richness and evenness in the NW Mediterranean Sea explored by pyrosequencing of the 16S rRNA. *Aquat Microb Ecol.* 2010; 61: 221-233.
- 785 75. David GM, López-García P, Moreira D, Alric B, Deschamps P, Bertolino P *et al.* Small freshwater ecosystems with dissimilar microbial communities exhibit similar temporal patterns. *Mol Ecol.* 2021; 30: 2162-2177.
76. Liu Y, Demina TA, Roux S, Aiewsakun P, Kazlauskas D, Simmonds P *et al.* Diversity, taxonomy, and evolution of archaeal viruses of the class Caudoviricetes. *PLoS Biol.* 2021; 19: e3001442.
- 790 77. Koonin EV, Dolja VV, Krupovic M, Varsani A, Wolf YI, Yutin N *et al.* Global organization and proposed megataxonomy of the virus world. *Microbiol Mol Biol Rev.* 2020; 84.
78. Shkoporov AN, Hill C. Bacteriophages of the Human Gut: The "known unknown" of the microbiome. *Cell Host & Microbe.* 2019; 25: 195-209.
- 795 79. Rezelj VV, Levi LI, Vignuzzi M. The defective component of viral populations. *Curr Opin Virol.* 2018; 33: 74-80.
80. Vignuzzi M, López CB. Defective viral genomes are key drivers of the virus–host interaction. *Nat Microbiol.* 2019; 4: 1075-1087.
- 800 81. Laurenceau R, Raho N, Forget M, Arellano AA, Chisholm SW. Frequency of mispackaging of *Prochlorococcus* DNA by cyanophage. *ISME J.* 2021; 15: 129-140.
82. Brussaard CP, Marie D, Bratbak G. Flow cytometric detection of viruses. *J Virol Methods.* 2000; 85: 175-182.
83. Zhang YZ, Chen YM, Wang W, Qin XC, Holmes EC. Expanding the RNA virosphere by unbiased metagenomics. *Annu Rev Virol.* 2019; 6: 119-139.
- 805 84. Dominguez-Huerta G, Zayed AA, Wainaina JM, Guo J, Tian F, Pratama AA *et al.* Diversity and ecological footprint of global ocean RNA viruses. *Science.* 2022; 376: 1202-1208.
85. Neri U, Wolf YI, Roux S, Camargo AP, Lee B, Kazlauskas D *et al.* Expansion of the global RNA virome reveals diverse clades of bacteriophages. *Cell.* 2022; 185: 4023-4037.e4018.
- 810 86. Edgar RC, Taylor J, Lin V, Altman T, Barbera P, Meleshko D *et al.* Petabase-scale sequence alignment catalyses viral discovery. *Nature.* 2022.
87. Menge DN, Weitz JS. Dangerous nutrients: evolution of phytoplankton resource uptake subject to virus attack. *J Theor Biol.* 2009; 257: 104-115.
- 815 88. Whitman WB, Coleman DC, Wiebe WJ. Prokaryotes: the unseen majority. *Proc Natl Acad Sci U S A.* 1998; 95: 6578-6583.
89. Takamiya H, Kouduka M, Suzuki Y. The deep rocky biosphere: New geomicrobiological insights and prospects. *Front Microbiol.* 2021; 12: 785743.

Fig.1. Estimated metagenome virus-microbe ratios (mVMR) across mock metagenomes with increasing VMR. **A**, Statistics of the different mock metagenomes generated with an increasing number of virus genomes (V000 to V125) as compared to the number of microbial cells (M00 – M01 – M10). **B**, Expected versus observed viral ratios versus cells (cells normalised to 1) in the different mock metagenomes as a function of the annotation method (OrfM vs. Prokka) used. Cells were counted using universal single copy genes (USCGs) and viruses using major capsid proteins (MCPs). **C**, Normalised counts (RPKM) of viruses per cell (normalised to 1) observed in mock metagenomes with our pipeline using OrfM and Prokka annotation strategies; a log₁₀ y-axis scale is used for a better discrimination in metagenomes where viral genomes were either absent or in very low abundance.

Fig.2. Strategies used to generate metagenomes in this study. Metagenomes from different planktonic fractions were obtained after sequential filtration of the same water mass, purification of DNA for each size fraction and proportional mixing per volume unit. For simplification, the intermediate filter of 20-30 µm pore-diameter size is not shown. Two metaviromes (particles <0.2 µm) were sequenced for control. Metagenomes of non-aquatic samples were generated after the in situ cell lysis and direct DNA purification prior to sequencing. EV, Etang des Vallées (freshwater system). * The metagenome WC-EdVall corresponds to the size fraction 50 kDa – 100 µm.

Fig.3. Epifluorescence- and normalised metagenome-based counts and ratios of cells and viruses in aquatic ecosystems. **A**, Flow-cytometry counts of cells and viral-like particles (VLPs) and estimated virus-to-microbe ratios (fVMR; histogram bars) from the same aquatic samples used to determine mVMR: EV, Etang des Vallées; MedS and MedD, 20 m and 40 m-deep Mediterranean plankton, respectively; Sal06 and Sal14, saltern ponds of 6 and 14% salinity (w/v), respectively. Sample names also indicate the plankton size fraction considered (Unf, all size fractions; <200, <100, <30 and <5, fractions below those numbers in µm; <0.2, fraction between 50 kDa and 0.2 µm; FE, final eluate <50 kDa). **B**, Normalised counts (RPKM) of viruses (MCPs) and cells (USCGs) from the three cellular domains metagenomes from the same original aquatic samples as in (A). Metagenomes correspond to size plankton fractions indicated by their suffixes: -all, fraction between 50 kDa and 200 µm (100 µm for EV); 02v, fraction between 50 kDa and 5 µm. Two metaviromes (fraction 50

kDa-0.2 μm) were sequenced for Mediterranean (MedS, MedD) plankton samples as internal
855 control. **C**, Metagenome-based normalised ratios of viruses per cell (bacteria + archaea +
eukaryotes). RPKM, reads per kilo base per million mapped metagenome reads. **D**,
Comparison of observed fMVR and mVMR for the same samples.

Fig. 4. Metagenome-based normalised ratios of viruses per cell across ecosystem types.

860 Viruses and cells were counted using, respectively, MCPs and USCGs as proxies; counts
were normalised to cell = 1. The lower panel corresponds to a zoom of the area shown within
a green rectangle in the upper panel. All the metagenomes were analysed using the same
pipeline from raw reads. Metagenome labels in the x-axis are coloured according to their
ecosystem type as indicated. RPKM, reads per kilo base per million mapped metagenome
865 reads.

**Fig. 5. Frequency of major cellular and viral taxa identified in all studied metagenomes
based on the phylogenetic assignment of USCG and MCPs.** Metagenome names are
coloured depending on their ecosystem type as indicated.

870

Fig. 6. mVMR and diversity parameters of cells and viruses per grand ecosystem type.

A, Boxplot showing the distribution of mVMR values; only significant differences are shown
($p < 0.001$). **B**, Boxplot showing the alpha diversity of cells and viruses; diversity differences
between cells and viruses were significant ($p < 0.0001$). **C**, Principal component analysis of
875 different metagenomes maximizing the variance explained by viruses (MCPs counts in
RPKM) and microbial cells (USCG counts in RPKM). Metagenomes are coloured as a
function of grand ecosystem type.

880

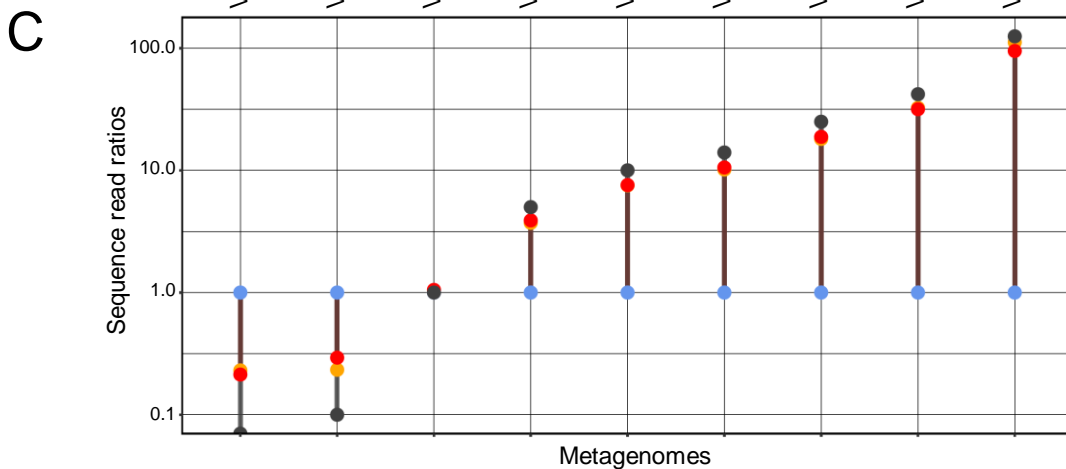
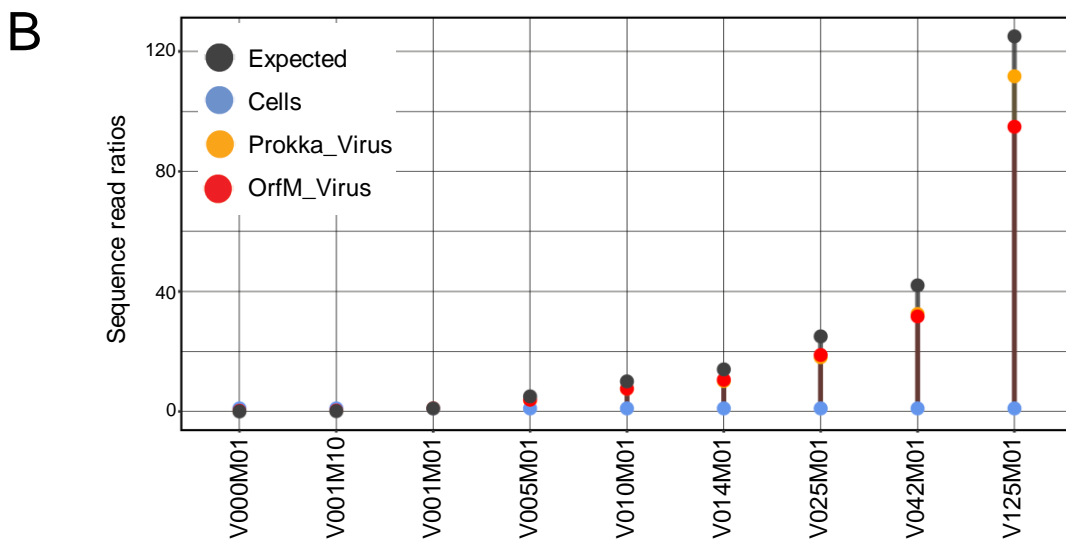
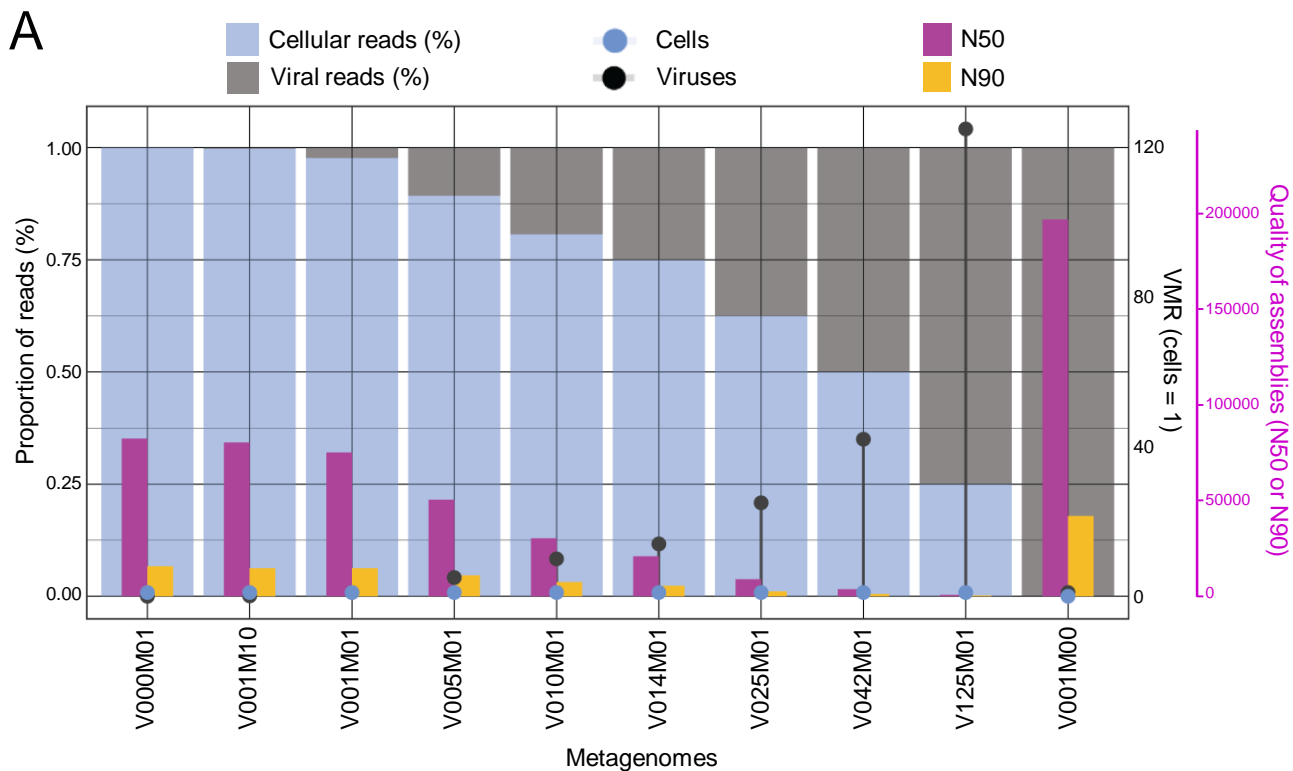


Fig. 1. Lopez-Garcia et al.

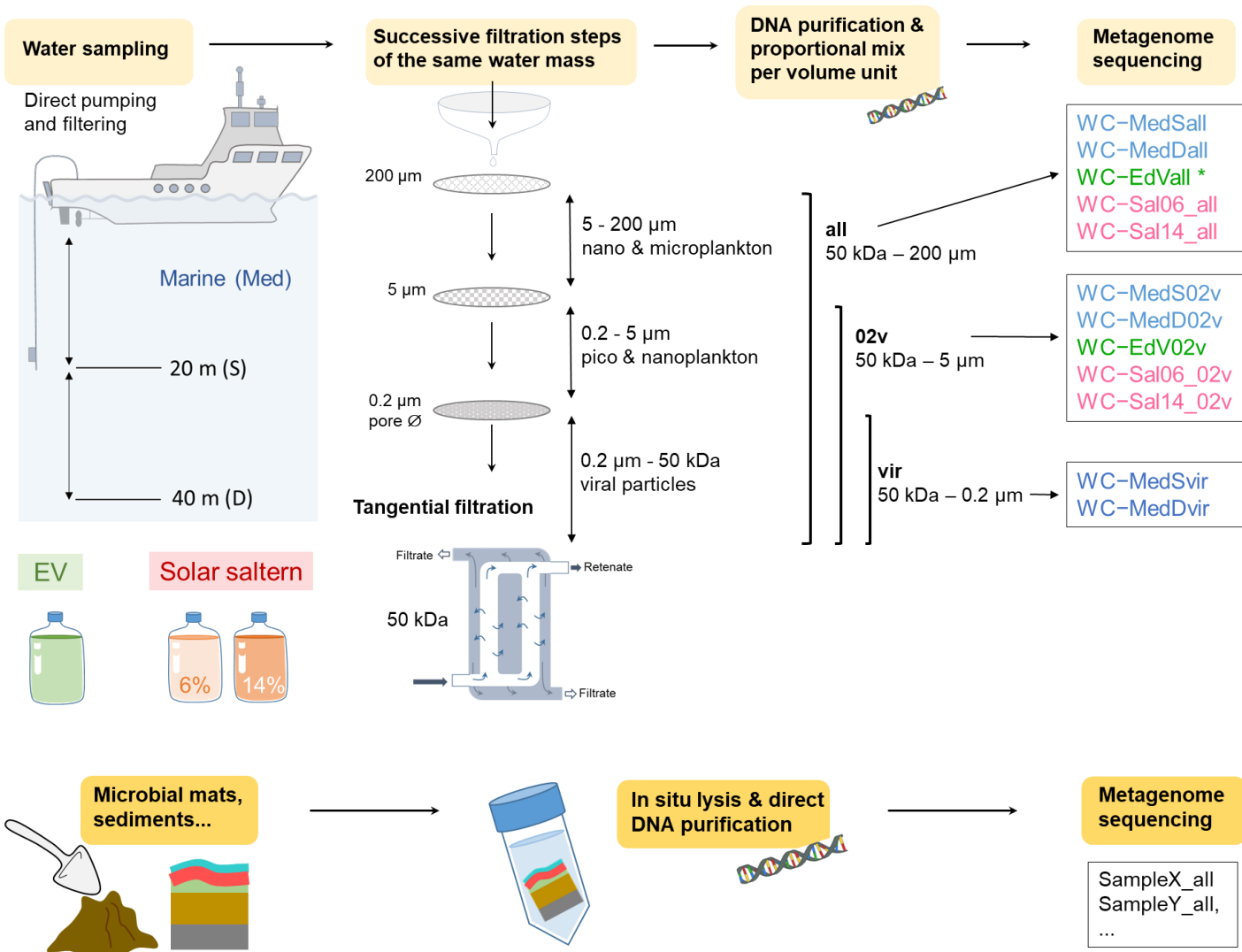


Fig. 2. Lopez-Garcia et al.

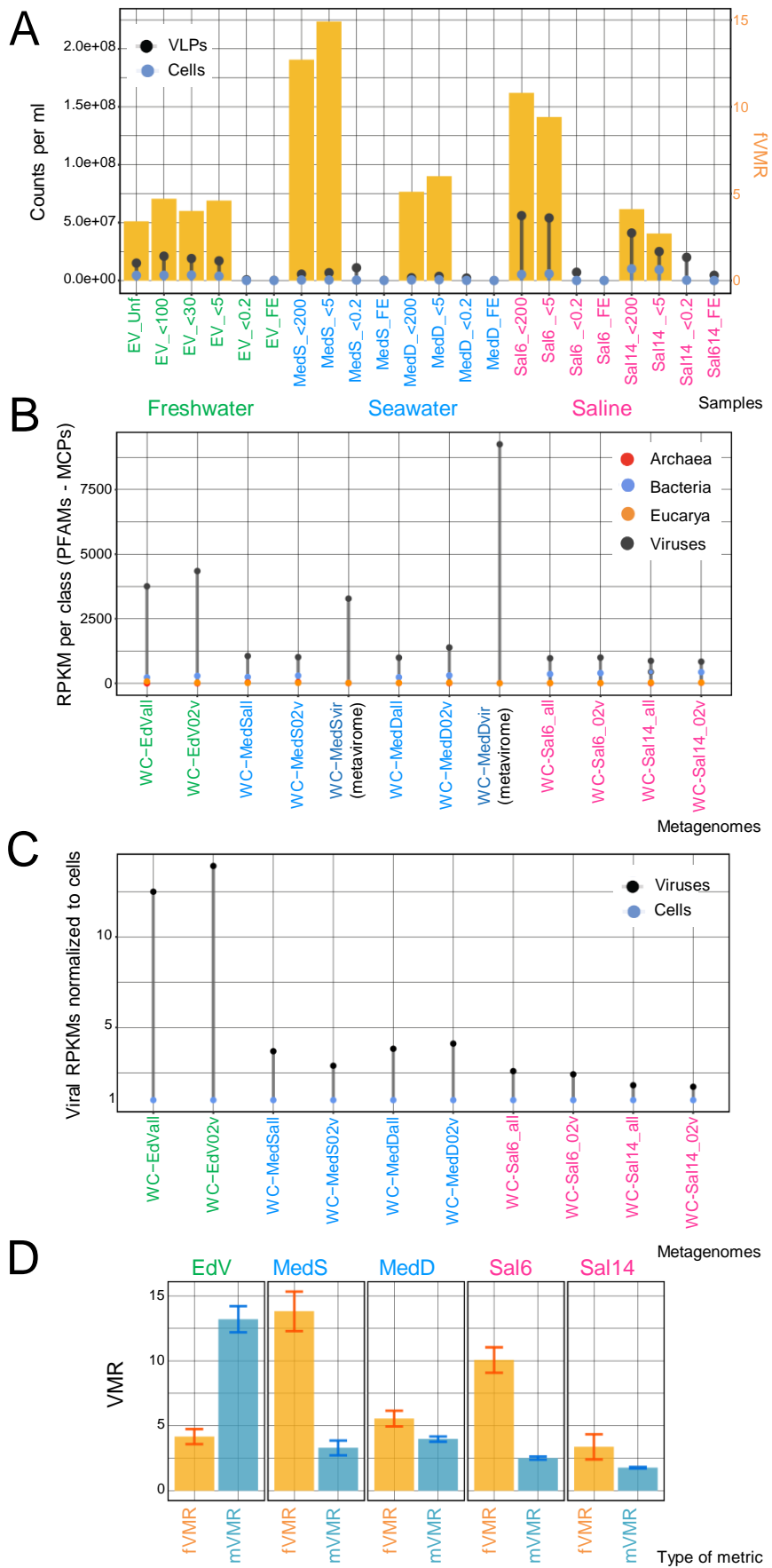


Fig. 3. Lopez-Garcia et al.

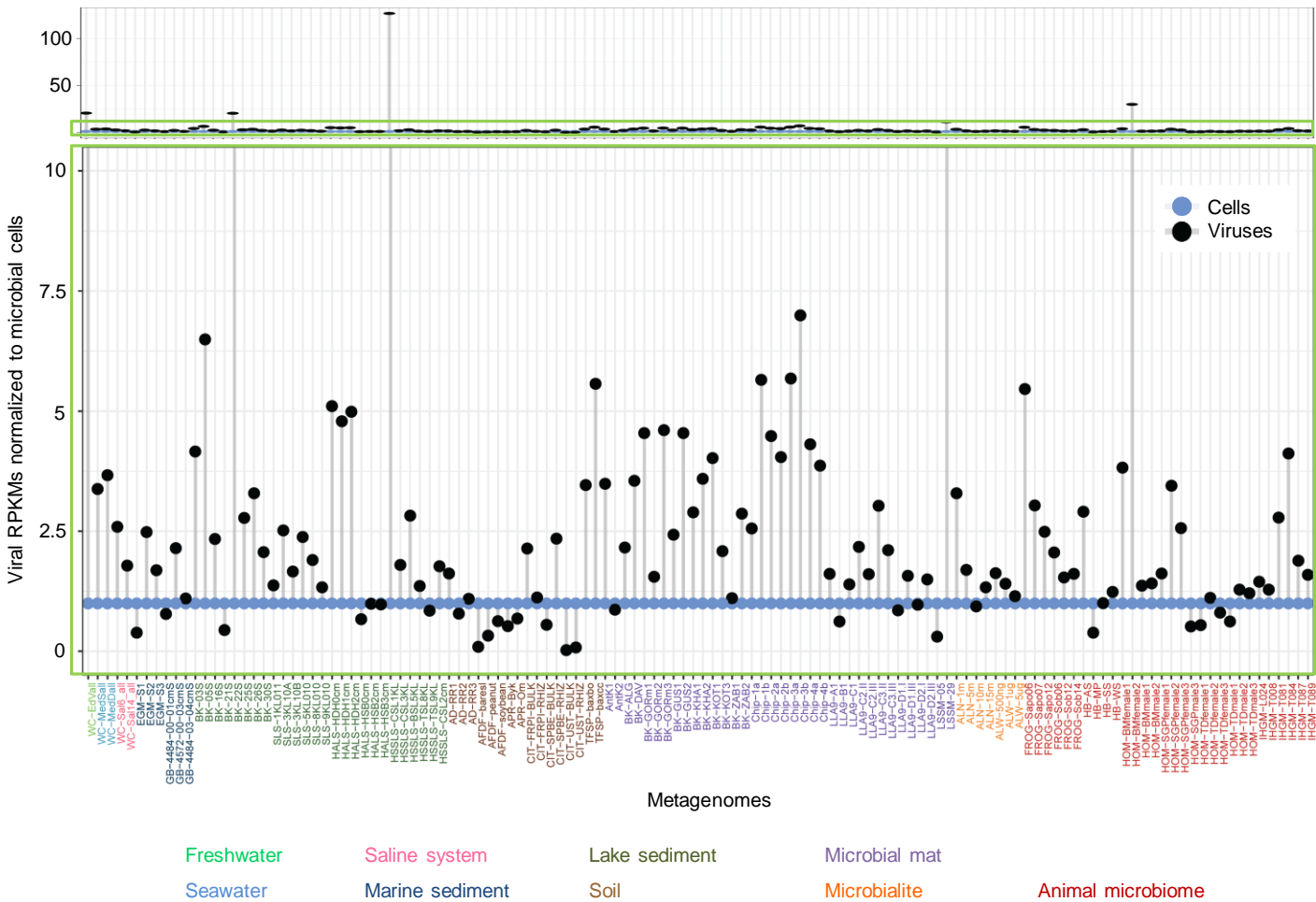
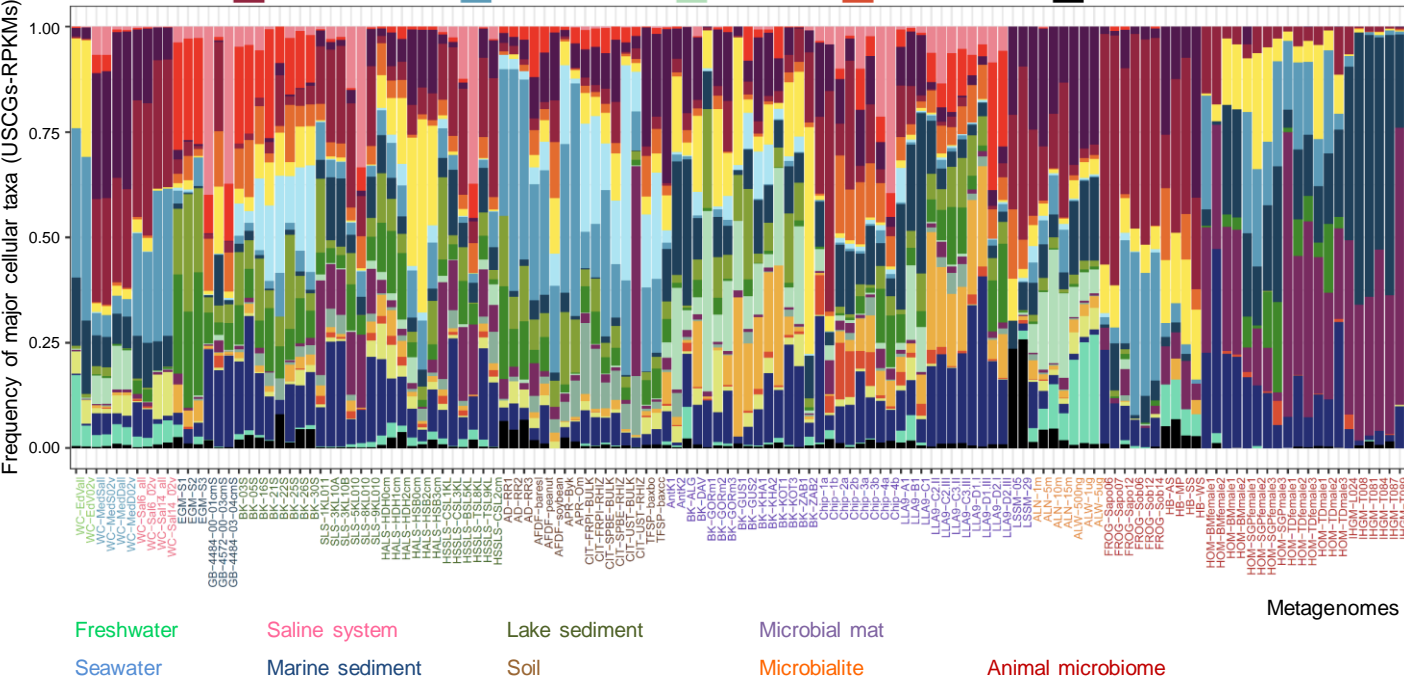
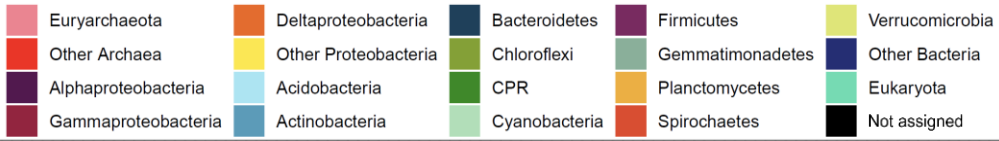


Fig. 4. Lopez-Garcia et al.

A



B

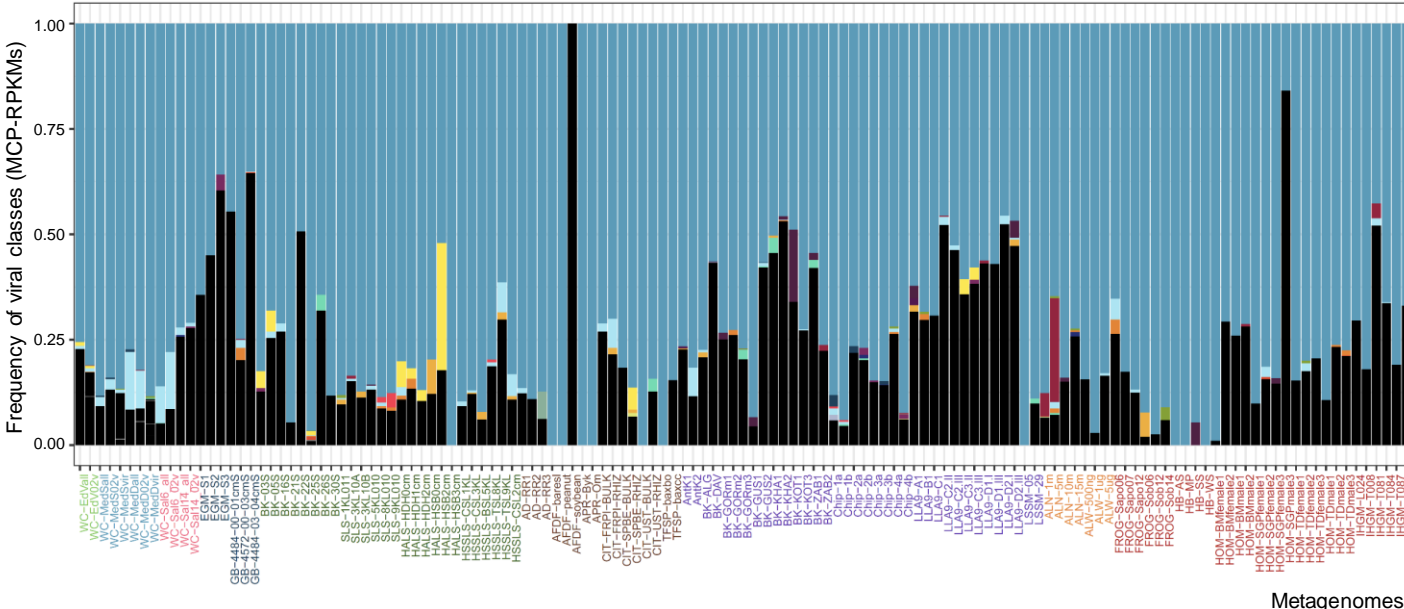


Fig. 5. Lopez-Garcia et al.

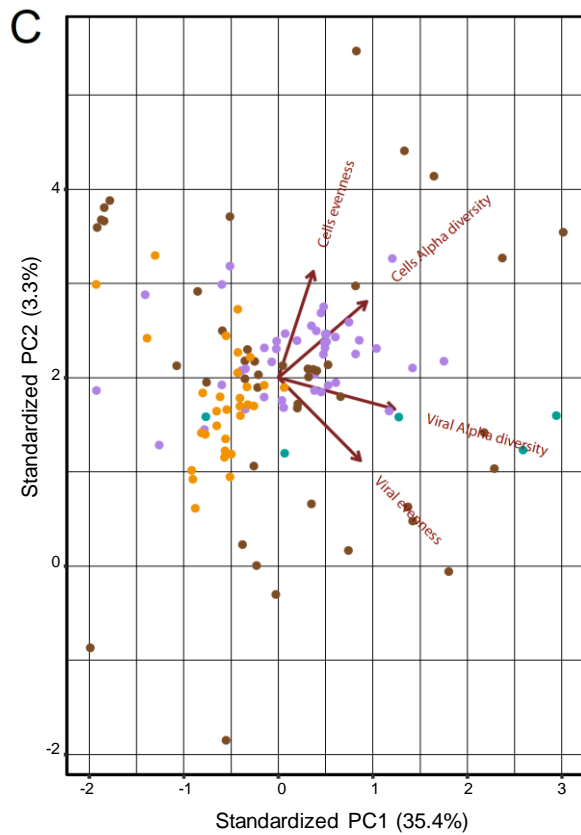
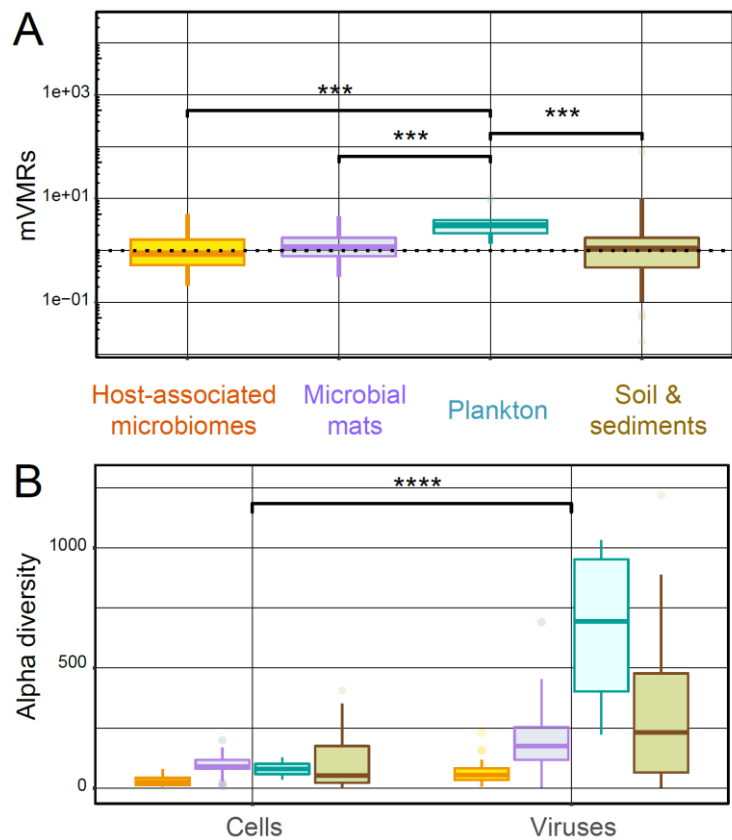


Fig. 6. Lopez-Garcia et al.